CHANDRA
X-ray Center 60 Garden St., Cambridge Massachusetts 02138 USA

MEMORANDUM

Date: April 17, 2000
From: M. Juda
To: Distribution
Subject: Corrections to HRC tap readouts
File: /data/juda1/juda/asc/hrc/tex/tap_correction.tex

1 Introduction

The HRC has a hardware problem that corrupts the data from the position taps under a specific set of conditions: the amplifier scale factor is switched to the least sensitive scale, an even number of taps on the axis have signals that are above a set threshold, and the event occurs on the negative side of the tap. When the above conditions are satisfied the tap signals are sampled while the amplifiers are still "ringing" after switching from the initial guess for the event coarse position to the correct one. The "ringing" results in offsets on the telemetered tap values from their true values, with the smallest signal of the triplet for an axis being the most affected. When the event position is calculated from the corrupted data, the positions are incorrectly determined and can be off by a few pixels. It may be possible to at least partially correct the effected data during ground processing. This memo describes the appearance of the corrupted tap data in the HRC-I and proposes a correction that can be applied to the tap with the smallest signal on an axis that is calculated from the other two tap values.

2 The Shape of Data

HRC event positions are calculated using the "3-tap" algorithm; the position of the event relative to the coarse position is given by:

$$X_{fine} = \frac{A_3 - A_1}{A_1 + A_2 + A_3}$$

where A_1, A_2, and A_3 are the signals from the three taps centered on the coarse position. Figure 1 is a scatter plot of fraction of the signal that is on the center tap versus this fine position for a subset of the events from an observation of Cas-A (OBSID 1409). The middle solid-line curve is a hyperbola that follows the locus of event points. The upper and lower solid-line curves are hyperbolas that are a bounding region for a screening test used to preferentially select x-ray events relative to background events or events that otherwise have poorly determined positions.

Figures 2 and 3 are similar plots for two other subsets from the same observation. The data for the three subsets are selected based on pulse height, which is a measure of the total charge collected on the position sensing grid. In both of the latter two cases, the locus of points on the positive fine position side follow the same curve as the data displayed in figure 1, while most of those on the negative side are systematically off of the hyperbola that describes the shape of good positions. Moreover, between figures 2 and 3 there are differences in their deviations from the locus of "good" points which depend on the size of the signal measured on the grid. One difference between the two to note is that the fine position at which the discontinuity off of the curve occurs becomes more negative as the pulse height increases. This effect can be explained by the fact that the "ringing" requires there to be an even number of taps exceeding a threshold and larger signals allow the events to occur farther away from the center of the tap before the number of taps above threshold changes from three to two.

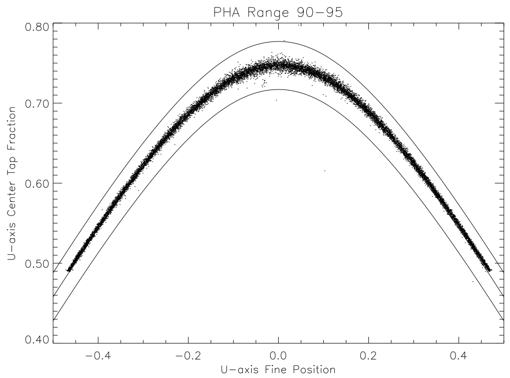

Figure 1: Plot of center tap fraction versus fine position for events showing the “hyperbolic” shape of the locus of well defined positions.

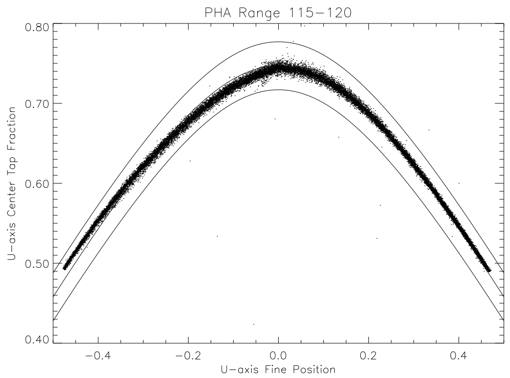

Figure 2: Plot of center tap fraction versus fine position for events showing the effect of “ringing” on the fine position calculation. This subset is from the lower end of the pulse height range of the affected data.

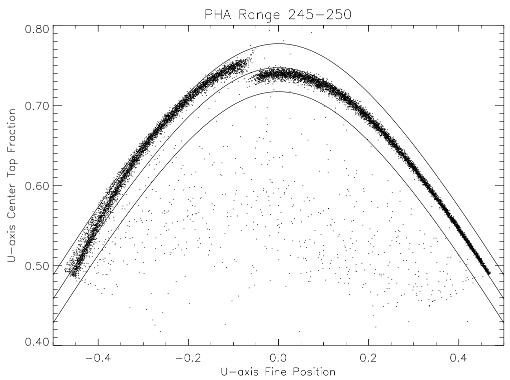

Figure 3: Plot of center tap fraction versus fine position for events showing the effect of “ringing” on the fine position calculation. This subset is from the upper end of the pulse height range of the affected data.

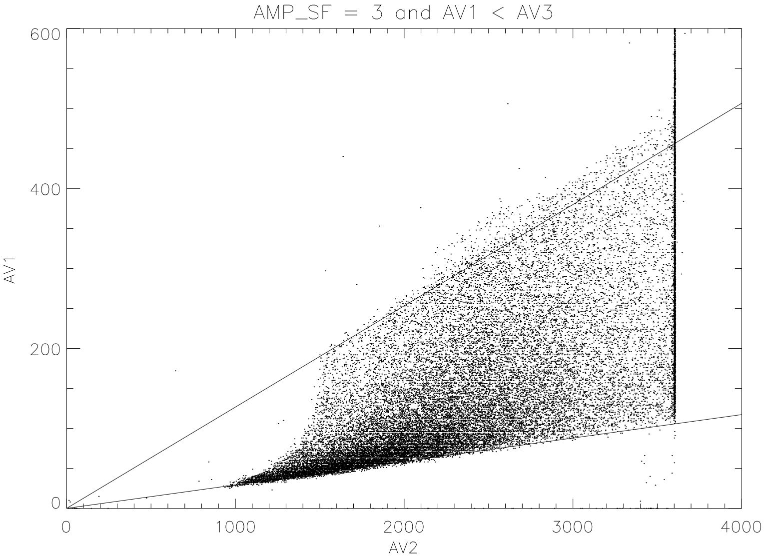

Figure 4: Plot of raw v-axis tap data for positive side of the taps.

The event data plotted in figures 1, 2, and 3 has already been somewhat processed; better insight into how the data is being corrupted can be obtained by plotting raw tap data. Plotted in figure 4 are raw v-axis tap data selected from the positive side of the central eight coarse positions (CRSV = 26-33, CRSU = 26-33) from the least sensitive amplifier scale (AMP_SF = 3). Only two of the three tap values are plotted; the abscissa is the central tap (i.e. the coarse position tap) signal, while the ordinate is the negative side tap signal (the one from the side opposite where the event occurred). The solid lines from the origin show the expected linear relationship between the tap values at the center and positive edge of the tap as the signals increase in amplitude. Figure 5 is a similar plot for the negative side of the taps with the ordinate being the tap signal from the positive side of the tap. The corruption of the tap

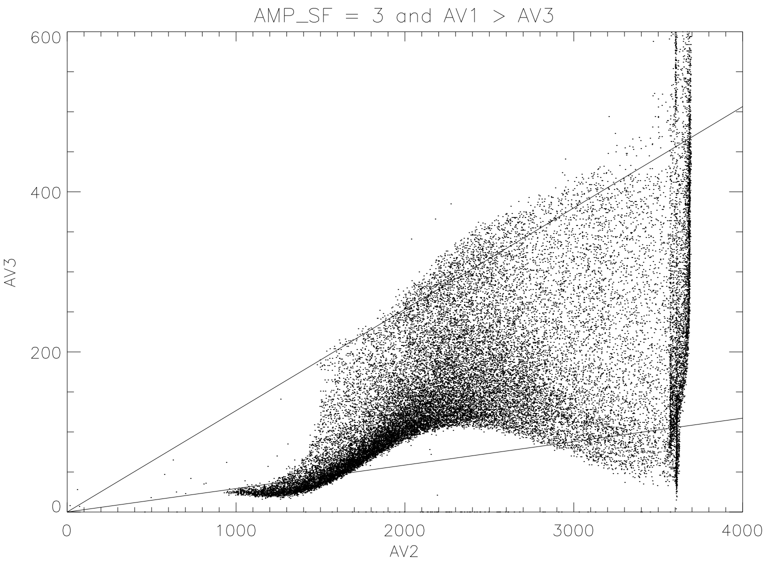

Figure 5: Plot of raw v-axis tap data for negative side of the taps.

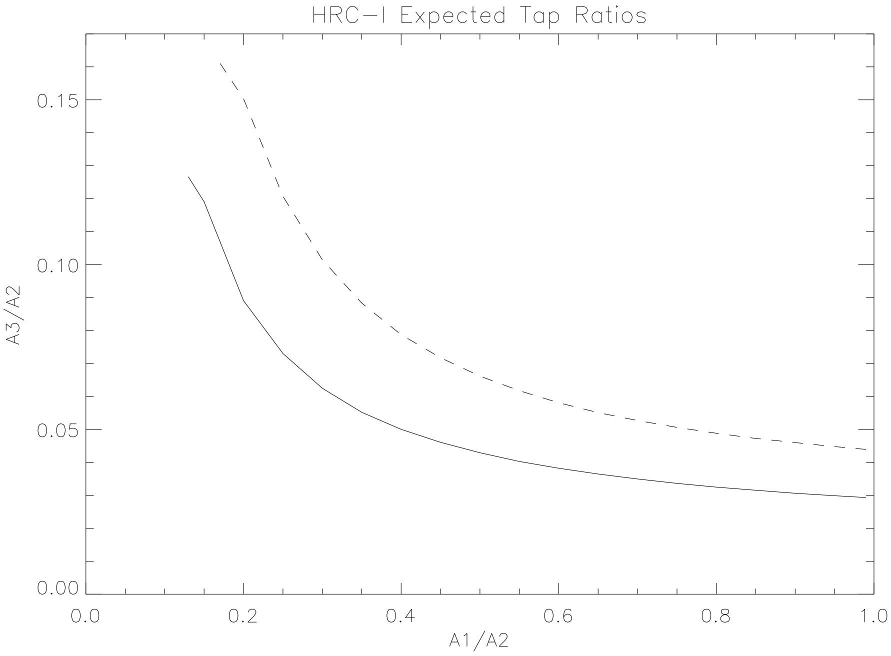

Figure 6: Relationship between tap ratios determined from events on the positive side of the taps. Solid curve: V-axis, Dashed curve: U-axis.

data for events occurring on the negative side of the tap can be seen as the sinusoidal pattern relative the expected linear relationship with increasing amplitude.

3 Sinusoidal Deviations

A better look at the sinusoidal distortion of the tap signal can be obtained by restricting the range of values of the third tap relative to the central tap This effectively restricts the events to a limited range of fine positions. With this selection of events it is also possible to remove the expected linear trend between the two tap values and observe the sinusoidal distortion directly. If we assume that the relationships between the tap signals should be symmetric across the tap, then the expected value for AV3/AV2 for a given AV1/AV2 range can be determined from the observed AV1/AV2 ratio for corresponding AV3/AV2 range on the good side of the tap. Figure 6 displays the expected relationships between the ratios of tap values for the two axes of the HRC-I.

Figure 7 shows the AV3 deviations from the expected value for only those events for which AV1/AV2 is in the range 0.98-1.00; these are the events near the negative edge of the tap. The amplitude of the sinusoid clearly increases with the size of the central tap signal (AV2). What is less obvious from the figure is that the sinusoid does not have a fixed period; the period appears to increase with increasing central tap signal. Also plotted in figure 7 is a sinusoid with amplitude and period that are linear functions of the center tap value:

$$\left(\frac{\mathrm{AV2}+b}{a}\right)\sin\left(2\pi\frac{\mathrm{AV2}-\phi}{c\mathrm{AV2}+d}\right).$$

The period function can be determined from the "zero crossing" points of the deviations from the expected value. The amplitude function can then determined from the observed deviations at AV2

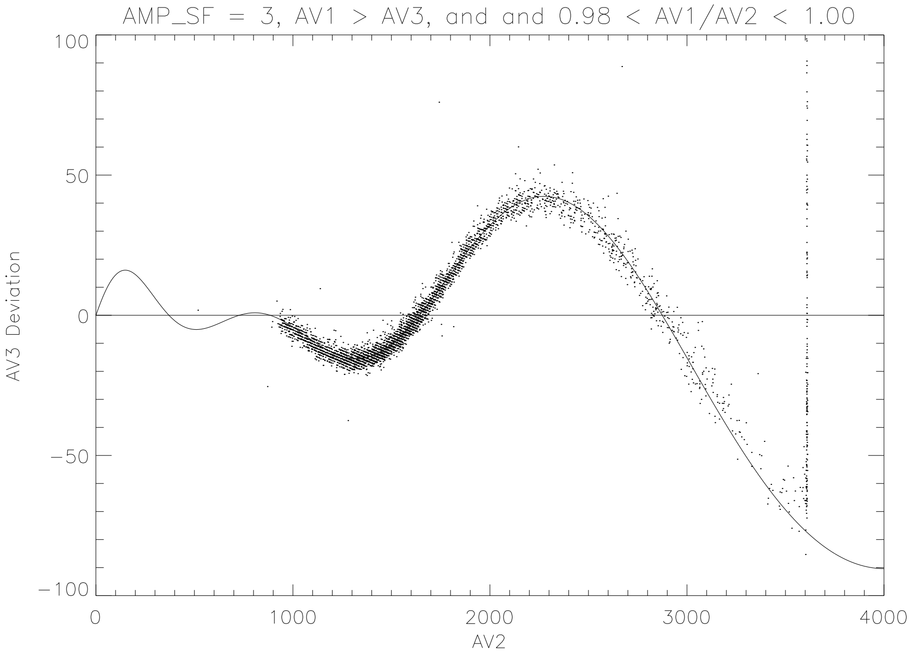

Figure 7: Plot of deviations of tap AV3 data from the expected value as a function of the signal on tap AV2 (expect AV3/AV2 = 0.0293).

Table 1: V-axis sinusoid coefficients

Coefficient	Value
a	-35.3
b	-728.0
c	0.278
d	638.0
ϕ	0.0

values where the sine function has a magnitude of 1. Since there are only two places where the sinusoid goes through zero, there is a multiplicity in period solutions depending on the phase adopted for the zero-crossing points (e.g. 1.0 and 1.5, 1.5 and 2.0, etc.) even after a value for ϕ is selected. For these data, a phase of 1.5 for the zero crossing at AV2 = $\sim$ 1640 appears to match the data reasonably well with an imposed constraint of $\phi = 0$. Table 3 lists the sinusoid coefficients used in this plot.

Figure 8 shows a similar plot for events with AV1/AV2 in the range 0.295-0.305. In this figure the sinusoid that is plotted with a dashed line is the same as the one in figure 7; clearly, the zero-crossing points have shifted. The sinusoid plotted with a solid line differs from the one plotted with a dashed line only by the value of ϕ (ϕ = 66). Since the zero-crossing points shift as AV1/AV2 changes, the sinusoid should be modified by making ϕ a function of AV1/AV2, ϕ(AV1/AV2).

Figure 9 is a plot of the lower of the two zero-crossing points as a function of AV1/AV2. The solid curve is a function of the form:

$$\alpha + \beta \left(\frac{1}{(\mathrm{AV1/AV2})^{\gamma}} - 1 \right),$$

with in this case: $\alpha = 1640$, $\beta = 75$, and $\gamma = 0.7$. The functional form of ϕ(AV1/AV2) is the same

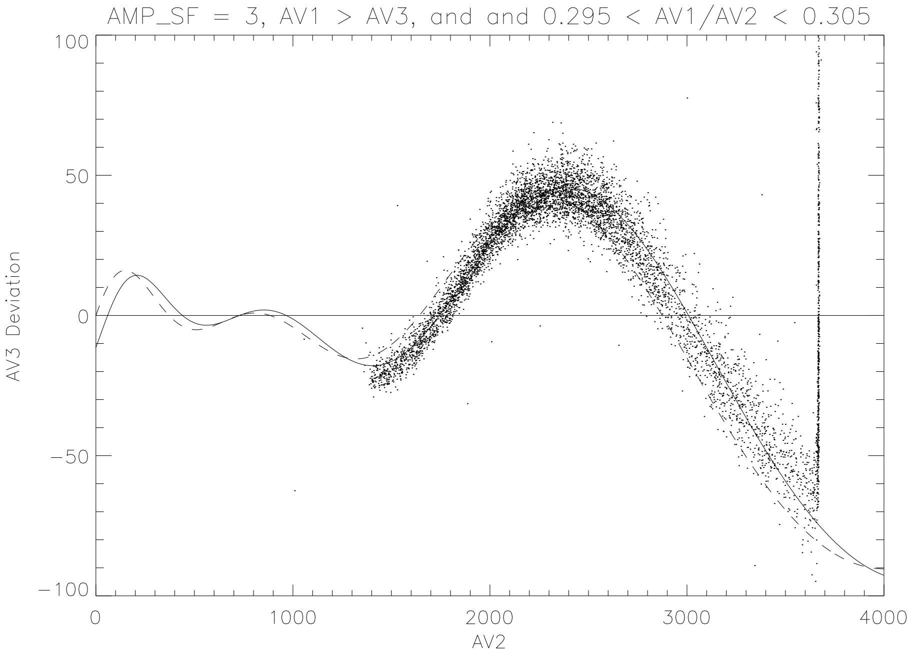

Figure 8: Plot of raw v-axis tap data for negative side of the taps. Data are selected to have $0.295 <$ $AV1/AV2 < 0.305$. The dashed curve is the same sinusoid as plotted in figure 7. The solid curve differs from the dashed curve only in the value of ϕ used in the sinusoid.

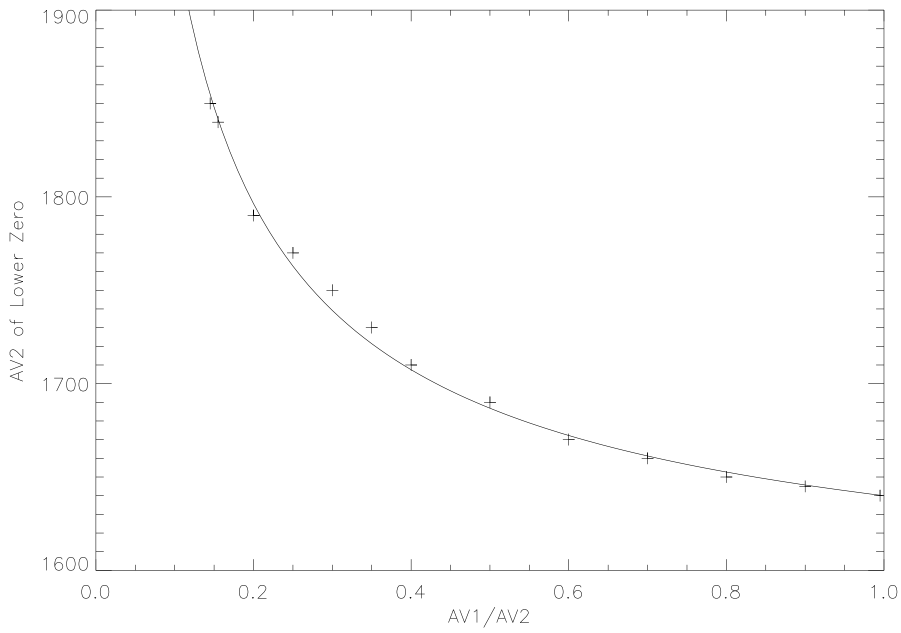

Figure 9: V-axis sinusoidal deviation lower zero-crossing point as a function of AV1/AV2.

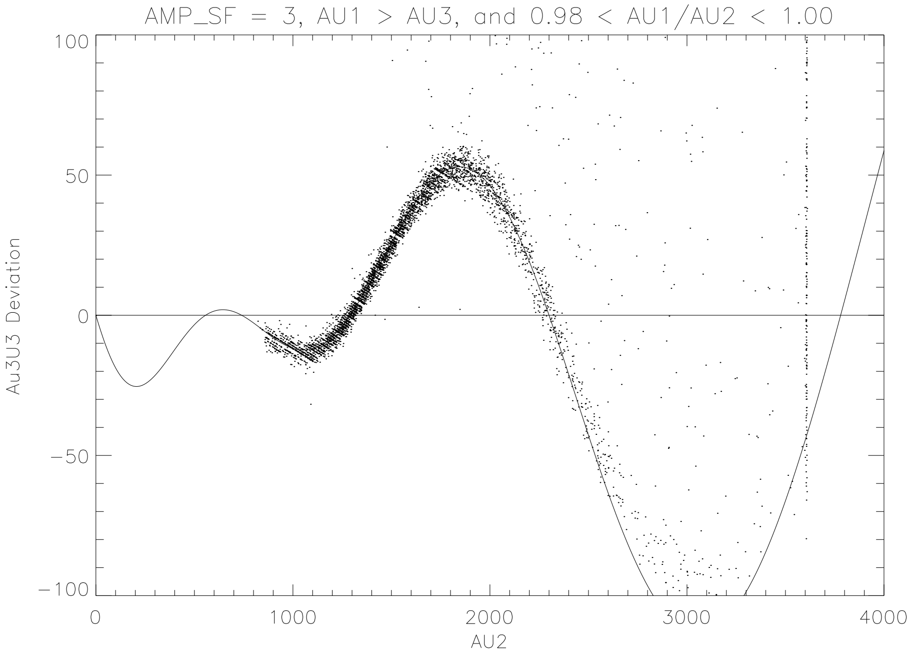

Figure 10: Plot of raw u-axis tap data for negative side of the taps. Data are selected to have AU1/AU2 in the range 0.98-1.00.

Table 2: U-axis sinusoid coefficients

Coefficient	Value
a	20.0
b	-740.0
c	0.241
d	979.0
ϕ	0.0

this curve but the constants α and β will change. Since we have determined the amplitude and period functions for the sinusoid from the AV1/AV2 ~ 1 range while imposing the constraint $\phi = 0$, then α is forced to be zero. The value of β is modified by the choice of the phase of this zero crossing point to be 1.5; $\beta = 75/1.5 = 50$. Thus we have:

$$\phi(\mathrm{AV1/AV2}) = 50((\mathrm{AV2/AV1})^{0.7} - 1)$$

The u-axis of the detector is affected as well and the sinusoid that matches the distortion can be found in a similar fashion. Figure 10 displays the u-axis data analogous to the v-axis data shown in figure 7. In this figure the data are selected to have AU1/AU2 in the range 0.98-1.00 so that they are from the negative edge of the tap. The coefficients of the sinusoid for the u-axis are different from those for the v-axis and are given in table 3. Again, in determining the sinusoid coefficients for these data, a constraint of $\phi = 0$ has been imposed. As with the V-axis, the sinusoid shifts in a systematic way as the AU1/AU2 selection range changes. Figure 11 shows how the lower zero-crossing point of the U-axis sinusoidal distortion changes with AU1/AU2. The solid curve has the same functional form as the curve in figure 9 but with $\alpha = 1290$, $\beta = 12$, and $\gamma = 2.0$.

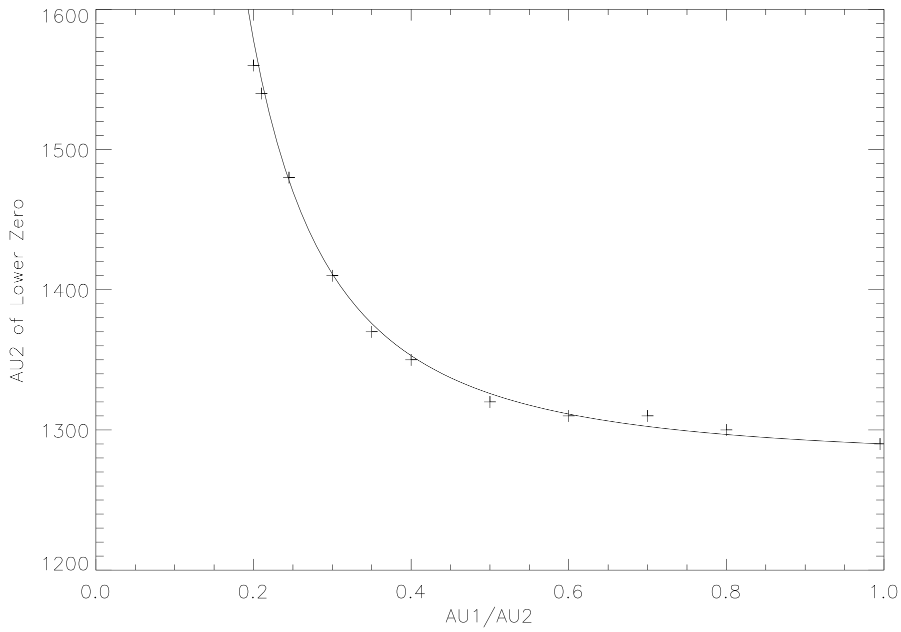

Figure 11: U-axis sinusoidal deviation lower zero-crossing point as a function of AU1/AU2.

4 Sinusoidal Corrections

The two sinusoid curves determined above can be used to correct the affected data on an event-by-event basis. The events that affected must meet the following conditions:

- AMP_SF = 3
- $A_1 > A_3$ for the axis - one or both can be affected
- $A_1 > constant \times A_2$ - the constant is different for each axis and could be zero.

Once the affected events are identified the corrupted tap value can be corrected:

$$\mathrm{A}_{3corrected} = \mathrm{A}_{3telemetered} - \left(\frac{\mathrm{A}_2 + b}{a}\right) \sin\left(2\pi \frac{\mathrm{A}_2 - \beta((\mathrm{A}_2/\mathrm{A}_1)^{\gamma} - 1)}{c\mathrm{A}_2 + d}\right)$$

Table 4 lists the values of the coefficients for sinusoids for both axes of the HRC-I along with the threshold on $\mathrm{A}_1/\mathrm{A}_2$ above which the correction should be applied.

This function form of the correction with the coefficients listed in table 4 was applied to an HRC-I observation of 3C273 (ObsID 461) as a test of this correction scheme. Figures 12 and 13 display the events from the negative side of the v-axis and u-axis taps respectively with the corrections applied to the affected events; in both cases the sinusoidal distortion is greatly diminished. Figure 12 can be compare directly to a "before" picture (from a different data set) in figure 5 and the raw data from the positive side of the v-axis taps in figure 4.

Figure 14 is an image of 3C273 produced using the corrected data and a linear degapping correction on each axis (U: 1.070, V 1.044). The data have been screened to reduce the background events and events with very poorly defined positions. The central image is more azimuthally symmetric than an image produced using the original data. Figure 15 gives the encircled fraction of events for the source versus radius in pixels.

Table 3: Sinusoid Correction Coefficients

Coefficient	V-axis	U-axis
a	-35.3	20.0
b	-728.0	-740.0
c	0.278	0.241
d	638.0	979.0
β	50.0	12.0
γ	0.7	2.0
A_1/A_2 threshold	0.14	0.20

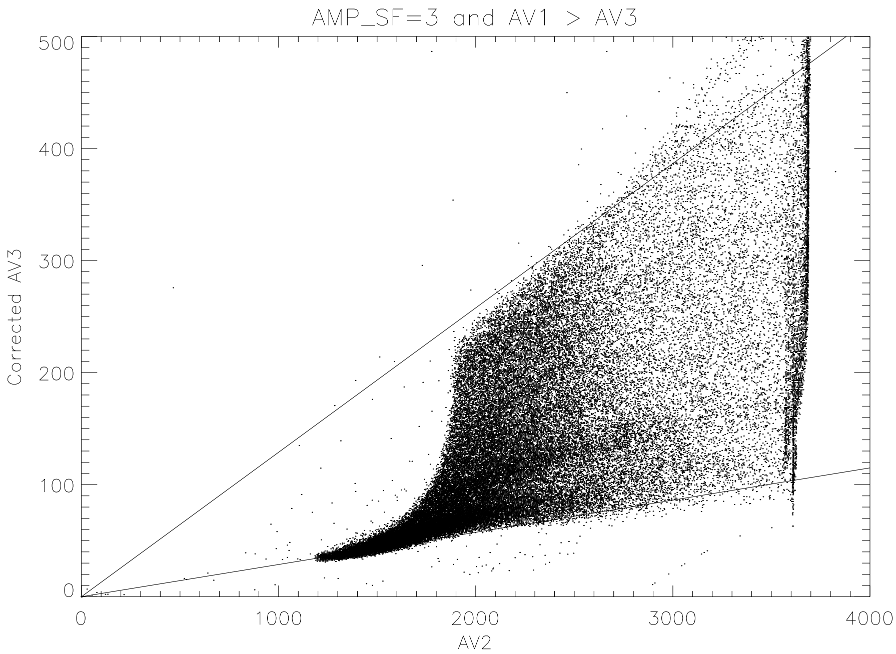

Figure 12: Plot of corrected v-axis tap data for negative side of the taps.

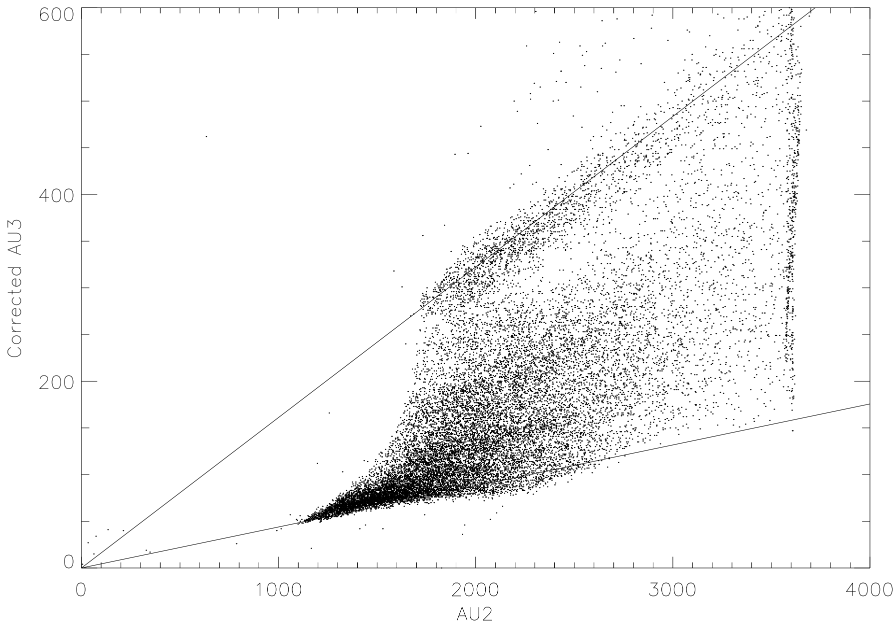

Figure 13: Plot of corrected u-axis tap data for negative side of the taps.

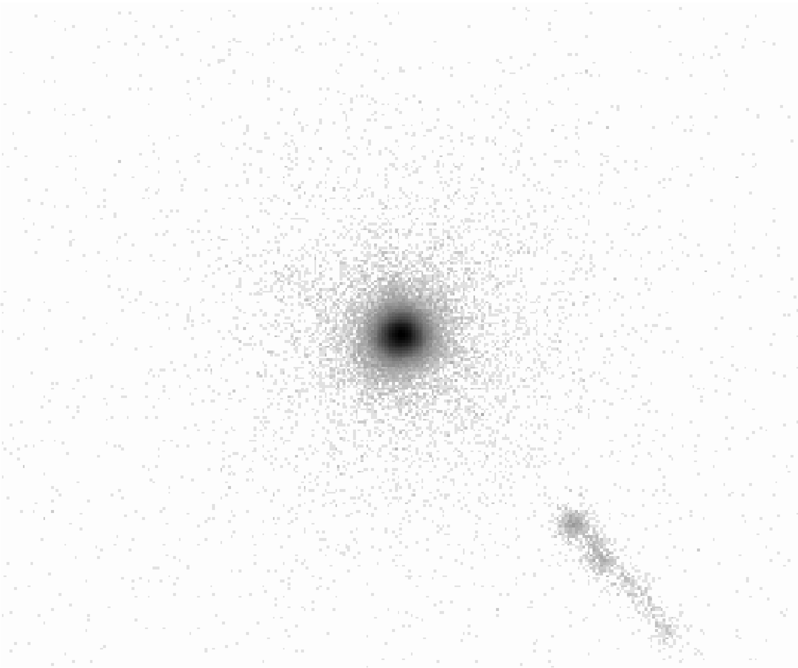

Figure 14: Image of 3C273 produced using corrected data. The data are displayed with a logarithmic intensity scale.

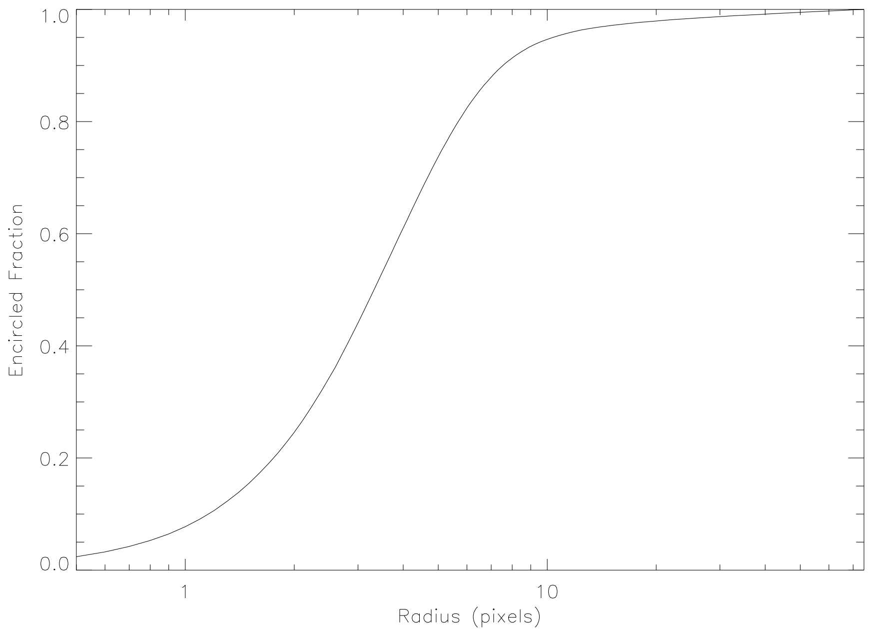

Figure 15: Encircled fraction of counts from 3C273 versus radius in pixels (1 pixel = ∼0.132 arcseconds).

5 Remaining Work

The algorithm for correcting the tap values is effective in improving the imaging performance of the HRC-I but there are still a few items that require more work. There may be some additional refinements to the coefficients to reduce the remaining residual deviations but the set given here are usable as a global set. It is possible that the coefficients could depend on the coarse position; this should be investigated. A set of coefficients need to be derived for the HRC-S.

Since the hardware cause for the ringing distortion is known, there is work in electrical engineering circuit modeling of the response of the HRC electronics. The modeled performance needs to be compared in detail to the laboratory version of the HRC electronics. It is possible that the knowledge gained from an improved understanding of the circuit performance can lead to a better algorithm for the correction, one that originates from first principles rather than being derived empirically.